Cresting the Coulomb Barrier of Polyanionic Metal Clusters

F. Martinez,[1] N. Iwe,[1] M. Müller,[2,1] K. Raspe,[1] L. Schweikhard,[2] J. Tiggesbäumker,[1,3,*] and K.-H. Meiwes-Broer[1,3]
[1]Institute of Physics, University of Rostock, 18059 Rostock, Germany
[2]Institute of Physics, University of Greifswald, 17489 Greifswald, Germany
[3]Department of Life, Light and Matter, University of Rostock, 18059 Rostock, Germany

(Received 18 April 2020; revised 20 November 2020; accepted 9 February 2021; published 29 March 2021)

Combining photoelectron spectroscopy with tunable laser pulse excitation allows us to characterize the Coulomb barrier potential of multiply negatively charged silver clusters. The spectra of mass- and charge-selected polyanionic systems, with $z = 2$–5 excess electrons, show a characteristic dependence on the excitation energy, which emphasizes the role of electron tunneling through the barrier. By evaluating experimental data from an 800-atom system, the electron yield is parametrized with respect to tunneling near the photoemission threshold. This analysis results in the first experimentally based potential energy functions of polyanionic metal clusters.

DOI: 10.1103/PhysRevLett.126.133001

Particles with diameters in the nanometer range exhibit a manifold of features that differ in many respects from those of the atom and the bulk. Prominent examples, also relevant for technical applications, are the exceptional reactivity of small gold nanoparticles [1] and the high optical absorption cross section of noble-metal quantum dots [2]. The origin of the substantial variety of physical and chemical properties can be traced back to the size dependence of the electronic level scheme. A basic question in this context is the impact of the cluster charge on bonding properties, especially when multiply charged anions are considered [3,4].

Molecular cluster polyanions in the gas phase have been studied extensively [5–9], leading to a comprehensive understanding of their electronic structure and ultrafast dynamics [10,11]. In polyanionic ligand-protected silver clusters, the photophysics appears to be governed by charge recombination through intersystem crossing on a femtosecond timescale [12]. Common to all polyanions is a potential energy surface characterized by a Coulomb barrier (CB [13]) with a height in the electronvolt range [3,14]. Because this barrier potential may stabilize molecular levels above the vacuum energy, it is responsible for negative electron affinities [7]. Note that the scenario resembles binding in metastable atomic nuclei with respect to α decay or proton emission.

In molecular systems, additional electrons are often located at defined sites. In contrast, clusters and nanoparticles of simple metals in a multiply negatively charged state provide various possibilities to explore correlated quantum objects. In other words, the study of jelliumlike clusters with delocalized valence electrons, as well as their response to additional charges will increase our understanding of the fundamental interactions in finite many-particle systems. This topic was first studied by conducting density functional calculations, including self-interaction correction, on small sodium clusters [15]. Outstanding problems with respect to the CB include competition between electron autodetachment and cluster fission [16,17] and the possibility of photoinduced two-electron emission from coinage metal cluster dianions [18].

Up to now, the study of polyanionic clusters (PAC) consisting only of metal atoms has focused mainly on charge-induced instability, e.g., Ref. [19]. In particular, experiments were directed at appearance sizes. Field emission through the CB turned out to be the reason for the low yields of Au_N^{z-} clusters of specific charges z and numbers of atoms N [20]. By modeling a barrier potential via combining the Coulomb repulsion with the attraction of an induced image charge, the stabilization of several electrons can be described qualitatively. However, for further analysis of the CB, the image-charge potential has a substantial drawback due to a singularity at the cluster surface. According to density functional calculations on Na_{18}^{2-} and C_{60}^{2-}, the potential at the cluster surface is expected to be smooth [21,22]. To date, however, no direct experimental observation of the confining potential $V(r)$ in metallic PAC exists. Such observations require consideration of the tunneling effect, with a transmission probability that is strongly dependent on the shape of the potential, especially at the cluster surface. Filling this knowledge gap is crucial for addressing the transition from the inner to the outer cluster potential, i.e., exploring the link between quantum mechanical binding and Coulomb repulsion.

For this Letter, we prepared size-selected silver clusters, decorated with a defined number z of excess electrons, i.e., Ag_N^{z-}. The charge-dependent $V(r)$ is deduced from a model-based analysis of photoelectron spectra (PES) recorded by scanning laser wavelengths in small steps.

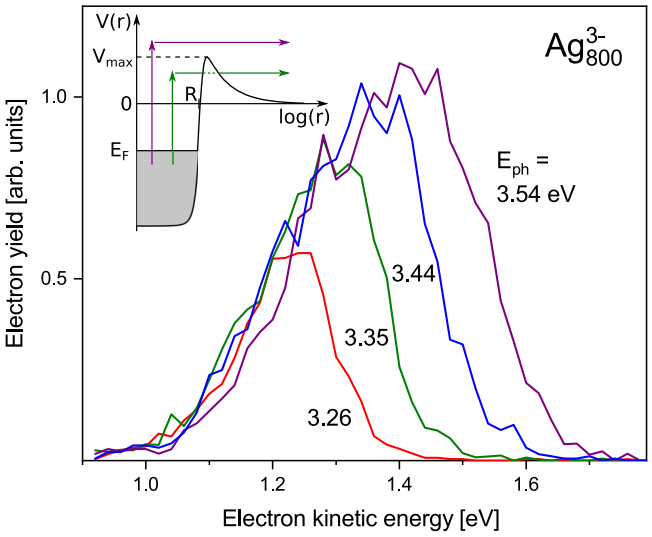

FIG. 1. Photoelectron spectra of Ag^{3-}_{800} for different laser photon energies E_{ph}. The shown yields are Y/S, i.e. normalized by S to account for absorption-dependent effects, for details see text. The common signal onset and the strong increase in the yields with E_{ph} indicates tunneling through the Coulomb barrier. Inset: The excess electrons in the PAC lead to the formation of a Coulomb barrier at the cluster surface. Direct photoemission from the electronic level system (shaded grey), as well as tunneling, may contribute to the spectra.

Because details of the experimental setup and the procedure to conduct photoelectron spectroscopy on metallic PAC will be published elsewhere, they are described only briefly here: The multiply charged target anions, Ag^{z-}_N, are generated by applying three-state digital ion trapping [23] to mass-selected silver cluster anions Ag^-_N and subsequent in-trap electron attachment [24]. The experimental cycle duration is mainly determined by the several hundred milliseconds required to successively charge the clusters, yielding overall repetition rates as low as 1 Hz. Pulsed extraction of Ag^{z-}_N from the ion trap into a drift tube leads to charge separation of the polyanions. In the laser interaction region, the PAC are exposed to wavelength-tunable nanosecond pulses from an optical parametric oscillator. Low pulse energies of about 10 μJ have to be chosen to minimize multiple absorptions. The photoelectron energies are determined by a magnetic bottle time-of-flight spectrometer with a transmission down to 0.15 eV. Because of the broad range of the electrons' kinetic energies E_{kin}, an extensive calibration of the spectrometer by ionization of atoms and photodetachment of small anionic clusters turned out to be essential. Moreover, the transmission function of the instrument was verified to be sufficiently constant; see Supplemental Material [25]. The PES shown here result from accumulation of typically 500–1000 experimental cycles and subsequent conversion of time of flight into energy spectra.

As an example, Fig. 1 depicts a series of PES from Ag^{3-}_{800} recorded at photon energies $E_{ph} = 3.26$ to 3.54 eV. The spectra, each consisting of a single peak, display a maximum and right slope that shift toward higher E_{kin} as E_{ph} increases. Obviously, the right-hand wings correspond to excitation from the upper occupied electronic levels (inset to Fig. 1). The onsets of the low-energy electrons, on the other hand, exhibit a common rise. This feature is attributed to the reduced transmission in the tunneling regime, which yields a lower signal strength when compared to direct emission. In Fig. 1, the transition from tunneling to direct emission is observed when adjusting E_{ph} from 3.44 to 3.54 eV. While the peak becomes broader, the maximum electron yield hardly changes, in contrast to the spectra for smaller E_{ph} where the signal is strongly suppressed. Hence, by tuning E_{ph}, the Coulomb barrier is incrementally crested.

In order to describe the PES of clusters as large as $N = 800$ at finite temperature, we assume a continuous level occupation with a distinct edge, characterized by a Fermi-Dirac distribution F_D. Density functional calculations show that the level separation in, e.g., Na_{198} already drops into the meV range [26], so the application of a smooth function F_D to model the right-hand wings is justified. The left-hand slopes of the spectra in Fig. 1 are considered to originate solely from the depressed transmission through the CB that is determined by the energy-dependent electron tunneling probability $P(E_{kin})$. Note, that both F_D and P scale nearly exponentially with E_{kin}, and thus they should lead to characteristic high- and low-energy drops in the spectra. Indeed, when plotting the yields of Fig. 1 on a logarithmic scale, the respective slopes become almost straight lines, as shown in Fig. 2 for Ag^{3-}_{800} as well as the other charge states under investigation.

In the following, we set up a model that considers only the tunneling process and supposes a dense level occupation close to the "Fermi" energy. Fitting the model to measured PES will allow us to deduce details of $V(r)$, assuming that the normalized photoelectron yields Y/S are affected only by the transmission above and through the barrier. Because of the large cluster size, the system can be approximated by an ideal metallic droplet of radius $R = r_s N^{1/3}$, with the Wigner–Seitz radius $r_s = 1.6$ Å for silver [27]. The photoemission of a z-fold charged PAC,

$$M^{z-}_N + h\nu \rightarrow M^{(z-1)-}_N + e^-, \quad (1)$$

is described by an electron departing the Coulomb field of the remaining (z-1)-charged cluster. The resulting electron yield is the product of three contributions:

$$Y = S(E_{ph}) \cdot F_D(E_{kin} - E_{ph}, T) \cdot P[E_{kin}, V(r)], \quad (2)$$

(i) a scaling factor S incorporating wavelength-dependent laser intensities and absorption cross sections.

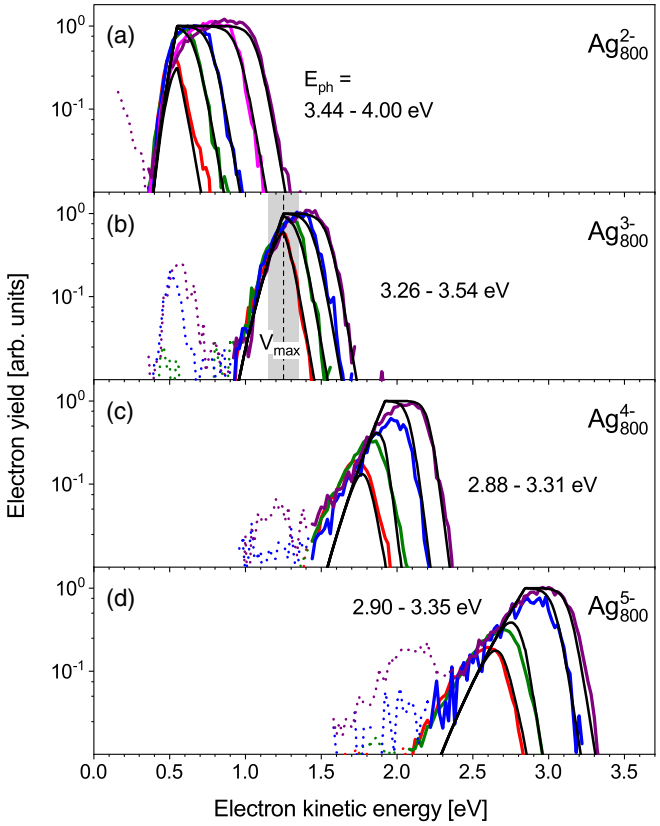

FIG. 2. PES of Ag_{800}^{z-}, $z = 2$–5 (colored lines), with laser excitation energies as indicated. All curves are displayed on a logarithmic scale and normalized with respect to S. Plotting Eq. (2) with the mean values of ε and T from the fits to the measured PES (Table I) results in the black curves. Figure 2(b) shows the respective data of Fig. 1, with the vertical dashed line denoting exemplarily the extracted Coulomb barrier height $V_{\max}$ with its uncertainty range marked in grey. Multi-photon absorption-induced photoemission cannot completely be suppressed, as seen by the dotted contributions.

(ii) the Fermi–Dirac distribution F_D, with T being the temperature of the cluster. The Fermi energy E_F denotes the position of the uppermost occupied level with respect to the vacuum energy (inset to Fig. 1). For a given photon energy, the corresponding E_{kin} is identified from the steepest slope in the right-hand wing of the measured photoelectron curve. Energy conservation determines the Fermi level, e.g., $E_F = -2.00(5)$ eV for Ag_{800}^{3-}.

(iii) the tunneling probability P, which is based on a number of assumptions. First, the clusters are considered to be spherical, although a refined approach may require charge-dependent deformations. Second, the single-particle potential $V(r)$ is modeled by a superposition of two functions:

$$V(r) = V_C(r) + V_{\mathrm{WS}}(r). \tag{3}$$

The first term specifies the electrostatic potential V_C, which is given by a $(z-1)$-fold point charge outside the residual PAC ($r \geq R$), while it is kept constant inside. At the cluster radius R a tiny kink results, which, however, is insignificant as it is hidden by the steep drop of the overall potential, $V(r)$. For the second part we choose the Woods-Saxon potential $V_{\mathrm{WS}}(r)$,

$$V_{\mathrm{WS}}(r) = -V_0\left(1 + \exp\left(\frac{r-R}{\varepsilon}\right)\right)^{-1}, \tag{4}$$

where the well depth is given by V_0 and the surface smoothness by ε. This phenomenological potential from nuclear physics nicely parameterizes the many-body quantum solution of an ideal metallic system [28]. V_0 is taken as the sum of the ionization energy of the neutral cluster (4.78 eV) [29] and of an assumed width of the occupied cluster levels of 3 eV [26]. The inset to Fig. 1 illustrates $V(r)$, showing a pronounced CB. For a given charge state, the barrier height $V_{\max}$ is determined by both parameters in Eq. (4), V_0 and ε, where one counteracts the influence of the other. As V_0 has already been estimated, only ε remains to be extracted from the experimental data. Indeed, varying V_0 has a negligible effect on the barrier heights obtained from the fit procedures. Using the potential $V(r)$ constructed in Eq. (3), the tunneling probability P is calculated for an electron within the Wentzel-Kramers-Brillouin approximation

$$P[E_{\mathrm{kin}}, V(r)] = \exp\left[-\int_{r_1}^{r_2}\sqrt{\frac{8m_e}{\hbar^2}[V(r) - E_{\mathrm{kin}}]}dr\right], \tag{5}$$

with r_1, r_2 given by $V(r_1) = V(r_2) = E_{\mathrm{kin}}$ [30].

Fitting the experimental PES of Ag_{800}^{z-} with Eq. (2) produces a set of parameters: the potential smoothness ε, the cluster temperature T, and the scaling factor S. The experimental spectra have been normalized to their respective S to compensate for the wavelength-dependent cross sections, e.g., due to plasmons [31]; see the Supplemental Material [25]. Within each charge state z, the values of ε and T show minor variations with E_{ph}. Therefore, and for a clear presentation, respective mean values for ε and T (Table I) enter Eq. (2) to jointly model the spectra, see the black curves in Fig. 2. All fits reproduce the general trend of the experimental PES, including the spectral shifts due to the charging energy. Interestingly the left-hand sides of the spectra show slopes which significantly decrease with increasing z. In fact, this may be a valid signature for tunneling, because the higher the charge state, the larger the CB height, which results in a tunneling probability function $P(E)$ whose interval $P = [0; 1]$ has to be stretched over a, respectively, larger energy range, $E = [0; V_{\max}]$. Low-energy parts observed in the spectra (dotted) originate from secondary photoabsorption of the $(z\text{-}1)$ polyanion and consecutive electron emission. Those contributions can also be reproduced by our model, as demonstrated in the Supplemental Material [25].

TABLE I. Mean values of surface smoothness ε and cluster temperature T extracted from the fits to the measured PES for $z = 2$–5, as well as the corresponding barrier heights $V_{\max}$.

z	ε/Å	T/K	$V_{\max}$/eV
2	1.8 ± 0.7	480 ± 100	0.55 ± 0.10
3	1.5 ± 0.4	470 ± 70	1.25 ± 0.10
4	1.5 ± 0.4	340 ± 70	1.92 ± 0.15
5	1.1 ± 0.6	430 ± 70	2.85 ± 0.30

In case of the higher charge states, i.e., Ag_{800}^{4-} and Ag_{800}^{5-} the fit procedure underestimates the yields of the left-hand wings. Note, that for these two datasets, a determination of S prior to the fitting procedure was required, for details see the Supplemental Material [25]. We attribute this weak deviation from our model to the onset of overlapping events from the low-energy parts (dotted) and to possible shape deformations, where the latter may have an impact on tunneling rates. Still, the overall agreement with the experimental spectra is rather convincing also for $z = 4$ and 5. The kinks in the fit curves mark the transition from tunneling to direct emission, i.e., they denote the height of the CB. This is indicated for Ag_{800}^{3-} by the dashed vertical line in Fig. 2(b). The extracted values for T of about 400 K seem reasonable since the electron attachment process in the trap takes place at room temperature and may heat the cluster.

Applying the analysis on Ag_{800}^{z-} leads to a corresponding potential curve $V(r)$ for each charge state $z = 2$–5 (Fig. 3). These single-particle potentials correspond to the $(z-1)$-fold charged systems remaining after photoemission, Eq. (1). A common feature of all $V(r)$ is the existence of a CB with a height $V_{\max}$ that increases with z. Classically, with a square-well potential ($\varepsilon \to 0$), $V_{\max}$ is located at the cluster radius ($R = 1.48$ nm for Ag_{800}), and it increases by steps defined by the charging energy of a metallic droplet ($k_C e^2/R = 0.97$ eV, where k_C is the Coulomb constant). This charging energy appears as bias of the potentials inside the cluster in Fig. 3. On the other hand, the steps of the experimentally derived values of $V_{\max}$ are around 0.7 eV, and the radial position of $V_{\max}$ depends on the charge state. Hence, even for these large systems the CB cannot be explained by classical considerations alone.

The smoothness parameter ε of the Woods-Saxon potential plays a crucial role in the fitting procedure. This is observed for, e.g., Ag_{800}^{3-} when comparing the barrier height of $V_{\max} = 1.25$ eV to the small energy range of 0.3 eV covered by the left-hand slopes of the PES in Fig. 2(b). By recording only the upper quarter of the barrier, the complete model potential is deduced from the highly sensitive P, which is substantially characterized by ε. For example, as the charge state increases, the smaller ε values (Table I) indicate that the steepness of V_{WS} also increases, reflecting a presumably complex interplay between the

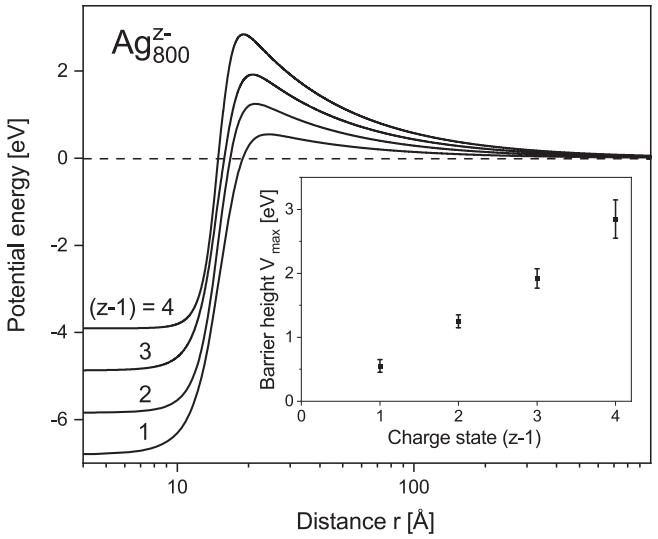

FIG. 3. Potentials $V(r)$ obtained from fitting the experimental spectra of Ag_{800}^{z-} with Eq. (2). These single-particle potentials correspond to the $(z-1)$-fold charged systems remaining after photoemission. The respective barrier heights $V_{\max}$ are compiled in the inset.

inner cluster potential and the excess charges. We note that our simplified ansatz neglects any photoemission dynamics. Centrifugal barriers were discussed [32], however, resulting Rydberg states have not been observed so far with metals in experiments. For solid surfaces, photoelectron emission was connected to the underlying statistics of the free electron gas within the Fowler-DuBridge model [33]. Furthermore, a possibly oscillating transmission coefficient as well as a more realistic density of electronic states may influence the yield close above the barrier top. Future investigations have to clarify whether these effects as well apply to the energy distribution, its width, and the quantum yield of large polyanionic metal clusters. Nevertheless, the experimental spectra shown here already reveal subtleties of the confining potential, opening up new anchor points for theoretical work.

CB heights have also been estimated from PES on molecular polyanions. In Refs. [34,35], $V_{\max}$ of the citric acid dianion resulted from the appearance of particular states in the spectra. In other studies, the CB heights were identified from spectral features, including CB-induced cutoffs [4,11,12] or low-energy electron onsets [9]. In contrast, we obtain values for the barrier heights that are independent of single spectral features or resonances. The finding strengthens the well-established assumption that metal clusters are ideal test grounds for the study of delocalized electron ensembles. With the possibility of tuning their size and preparing several anionic states, they provide a variety of Coulomb barriers to explore. This new parameter landscape opens up exciting routes to tackle issues relevant to other areas of research. For example, the phenomenon of tunneling delay is still under discussion [36].

In contrast to intense laser pulse experiments [37], where the tunneling conditions develop in the strong laser field, the CB is a feature of the initial metal cluster system. Hence, analyzing the response of PAC to sculpted laser pulse excitation [38,39] may contribute to clarifying the dynamics of electron tunneling on attosecond timescales. Other fields like the physics of complex plasmas with negatively charged particles might also benefit from the knowledge of $V(r)$ including the complete Coulomb barrier [40]. Finally, it is conceivable that with ultrafast photoemission electron microscopy (PEEM) potential energy surfaces similar to those of the PAC can be obtained by adjusting the electrical field above a solid surface or nanoparticle. The evolution of the PEEM spectra for different photon energies could as well be dominated by both the electron tunneling and the occupation close to the Fermi level.

In conclusion, the first photoelectron spectra of polyanionic, pure metal clusters have been obtained for mass- and charge-state selected species. Investigation of the wavelength dependence provided access to details of Coulomb barriers. Evaluating the data in a model that combines a Woods-Saxon ansatz with the Coulomb potential to describe the impact of tunneling on the emission allowed the extraction of barrier heights and positions. Future studies will aim for a direct determination of the energy-dependent barrier widths from the observed tunneling rates. A goal is to obtain the potential shape without predefining functions for its attractive part. The relevance of the potential smoothness at the cluster surface has to be clarified through a comprehensive quantum treatment of this many-particle problem.

F. M. and N. I. contributed equally to this work. We acknowledge Christian Peltz, Thomas Fennel, Ingo Barke, and Dieter Bauer for helpful discussions about theoretical issues, as well as Steffi Bandelow for valuable hints on ion-trap technology. Stefan Lochbrunner provided us with the tunable laser system. Financial support has been granted by the German Research Foundation (DFG), within the SFB 652, TI210/ 10-1, and the Federal Ministry of Education and Research (05K16HR1). M. M. acknowledges support by the Int. Helmholtz Graduate School for Plasma Physics HEPP.

*josef.tiggesbaeumker@uni-rostock.de

[1] A. Sanchez, S. Abbet, U. Heiz, W.-D. Schneider, H. Häkkinen, R. N. Barnett, and U. Landman, When gold is not noble: Nanoscale gold catalysts, J. Phys. Chem. A **103**, 9573 (1999).

[2] J. Zheng, P. R. Nicovich, and R. M. Dickson, Highly fluorescent noble-metal quantum dots, Annu. Rev. Phys. Chem. **58**, 409 (2007).

[3] M. K. Scheller, R. N. Compton, and L. S. Cederbaum, Gas-phase multiply charged anions, Science **270**, 1160 (1995).

[4] X.-B. Wang and L.-S. Wang, Photoelectron spectroscopy of multiply charged anions, Annu. Rev. Phys. Chem. **60**, 105 (2009).

[5] S. N. Schauer, P. Williams, and R. N. Compton, Production of Small Doubly Charged Negative Carbon Cluster Ions by Sputtering, Phys. Rev. Lett. **65**, 625 (1990).

[6] P. A. Limbach, L. Schweikhard, K. A. Cowen, M. T. McDermott, A. G. Marshall, and J. V. Coe, Observation of the doubly charged, gas-phase fullerene anions C_{60}^{2-} and C_{70}^{2-}, J. Am. Chem. Soc. **113**, 6795 (1991).

[7] X.-B. Wang and L.-S. Wang, Observation of negative electron-binding energy in a molecule, Nature **400**, 245 (1999).

[8] C. Stoermer, J. Friedrich, and M. M. Kappes, Observation of multiply charged cluster anions upon pulsed UV laser ablation of metal surfaces under high vacuum, Int. J. Mass Spectrom. **206**, 63 (2001).

[9] M. Vonderach, M.-O. Winghart, L. MacAleese, F. Chirot, R. Antoine, Ph. Dugourd, P. Weis, O. Hampe, and M. M. Kappes, Conformer-selective photoelectron spectroscopy of α-lactalbumin derived multianions in the gas phase, Phys. Chem. Chem. Phys. **16**, 3007 (2014).

[10] D. A. Horke, A. S. Chatterley, and J. R. R. Verlet, Femtosecond photoelectron imaging of aligned polyanions: Probing molecular dynamics through the electron-anion Coulomb repulsion, J. Phys. Chem. Lett. **3**, 834 (2012).

[11] P. D. Dau, H.-T. Liu, J.-P. Yang, M.-O. Winghart, Th. J. A. Wolf, A.-N. Unterreiner, P. Weis, Y.-R. Miao, C.-G. Ning, M. M. Kappes, and L.-S. Wang, Resonant tunneling through the repulsive Coulomb barrier of a quadruply charged molecular anion, Phys. Rev. A **85**, 064503 (2012).

[12] A. P. Veenstra, L. Monzel, A. Baksi, J. Czekner, S. Lebedkin, E. K. Schneider, T. Pradeep, A.-N. Unterreiner, and M.-M. Kappes, Ultrafast intersystem crossing in isolated $Ag_{29}(BDT)_{12}^{3-}$ probed by time-resolved pump-probe photoelectron spectroscopy, J. Phys. Chem. Lett. **11**, 2675 (2020).

[13] In other studies, the barrier is called "repulsive Coulomb barrier" (RCB).

[14] R. N. Compton, A. A. Tuinman, C. E. Klots, M. R. Pederson, and D. C. Patton, Electron Attachment to a Negative Ion: $e + C_{84}^{-} \rightleftharpoons C_{84}^{-2}$, Phys. Rev. Lett. **78**, 4367 (1997).

[15] C. Yannouleas and U. Landman, Multiply charged anionic metal clusters, Chem. Phys. Lett. **210**, 437 (1993).

[16] Y. Tasaka, K. Nakamura, S. Malola, K. Hirata, K. Kim, K. Koyasu, H. Häkkinen, and T. Tsukuda, Electron binding in a superatom with a repulsive coulomb barrier: The case of $[Ag_{44}(SC_6H_3F_2)_{30}]^{4-}$ in the gas phase, J. Phys. Chem. Lett. **11**, 3069 (2020).

[17] S. König, A. Jankowski, G. Marx, L. Schweikhard, and M. Wolfram, Fission of Polyanionic Metal Clusters, Phys. Rev. Lett. **120**, 163001 (2018).

[18] A. Herlert and L. Schweikhard, Two-electron emission after photoexcitation of metal-cluster dianions, New J. Phys. **14**, 055015 (2012).

[19] C. Yannouleas, U. Landman, A. Herlert, and L. Schweikhard, Multiply Charged Metal Cluster Anions, Phys. Rev. Lett. **86**, 2996 (2001).

[20] F. Martinez, S. Bandelow, G. Marx, L. Schweikhard, and A. Vass, Abundances of tetra-, penta-, and hexa-anionic gold clusters, J. Phys. Chem. C **119**, 10949 (2015).
[21] C. Yannouleas and U. Landman, Shell-correction method for calculating the binding energy of metal clusters: Application to multiply charged anions, Phys. Rev. B **48**, 8376 (1993).
[22] C. Yannouleas and U. Landman, Stabilized-jellium description of neutral and multiply charged fullerenes, Chem. Phys. Lett. **217**, 175–185 (1994).
[23] S. Bandelow, G. Marx, and L. Schweikhard, The 3-state digital ion trap, Int. J. Mass Spectrom. **353**, 49 (2013).
[24] F. Martinez, S. Bandelow, G. Marx, L. Schweikhard, and A. Vass, Electron attachment to anionic clusters in ion traps, Hyperfine Interact. **236**, 19 (2015).
[25] See Supplemental Material at http://link.aps.org/supplemental/10.1103/PhysRevLett.126.133001 for details of the electron spectrometer transmission and on the numerical evaluation method.
[26] W. Ekardt, Work function of small metal particles: Self consistent spherical jellium-background model, Phys. Rev. B **29**, 1558 (1984).
[27] N. W. Ashcroft and N. D. Mermin, *Solid State Physics* (Holt, Rinehart and Winston, New York, 1976).
[28] W. D. Knight, K. Clemenger, W. A. de Heer, W. A. Saunders, M. Y. Chou, and M. L. Cohen, Electronic Shell Structure and Abundances of Sodium Clusters, Phys. Rev. Lett. **52**, 2141 (1984).
[29] G. Makov, A. Nitzan, and L. E. Brus, On the ionization potential of small metal and dielectric particles, J. Chem. Phys. **88**, 5076 (1988).
[30] P. K. Dubey, Effect of image force on emission of electrons from negatively charged solid particles, J. Phys. D **3**, 145 (1970).
[31] J. Tiggesbäumker, L. Köller, K.-H. Meiwes-Broer, and A. Liebsch, Blue shift of the Mie plasma frequency in Ag clusters and particles, Phys. Rev. A **48**, R1749 (1993).
[32] J.-P. Connerade and A. Ipatov, Centrifugal barrier effects in metallic clusters, J. Phys. B **31**, 2429 (1998).
[33] L. A. DuBridge, Theory of the energy distribution of photoelectrons, Phys. Rev. **43**, 727 (1933).
[34] L.-S. Wang, C.-F. Ding, X.-B. Wang, and J. B. Nicholas, Probing the Potential Barriers and Intramolecular Electrostatic Interactions in Free Doubly Charged Anions, Phys. Rev. Lett. **81**, 2667 (1998).
[35] X.-B. Wang, C.-F. Ding, and L.-S. Wang, Photodetachment Spectroscopy of a Doubly Charged Anion: Direct Observation of the Repulsive Coulomb Barrier, Phys. Rev. Lett. **81**, 3351 (1998).
[36] R. Landauer and Th. Martin, Barrier interaction time in tunneling, Rev. Mod. Phys. **66**, 217 (1994).
[37] A. S. Landsman and U. Keller, Attosecond science and the tunnelling time problem, Phys. Rep. **547**, 1 (2015).
[38] Th. Brabec and F. Krausz, Intense few-cycle laser fields: Frontiers of nonlinear optics, Rev. Mod. Phys. **72**, 545 (2000).
[39] S. Skruszewicz, J. Tiggesbäumker, K.-H. Meiwes-Broer, M. Arbeiter, Th. Fennel, and D. Bauer, Two-Color Strong-Field Photoelectron Spectroscopy and the Phase of the Phase, Phys. Rev. Lett. **115**, 043001 (2015).
[40] S. Misra and M. S. Sodha, Photoelectric electron emission from a charged spherical particle: Modified DuBridge theory, Can. J. Phys. **92**, 236 (2014).